Single pulse emission from PSR B0809+74 at 150 MHz using Polish LOFAR station

Rahul Basu ®,[1]⋆ Wojciech Lewandowski ®,[1]⋆ Jarosław Kijak,[1]⋆ Śmierciak Bartosz,[2] Marian Soida,[2] Leszek Błaszkiewicz[3] and Andrzej Krankowski[3]

[1]*Janusz Gil Institute of Astronomy, University of Zielona Góra, ul. Szafrana 2, PL-65-516 Zielona Góra, Poland*
[2]*Astronomical Observatory of the Jagiellonian University, ul. Orla 171, PL-30-244 Kraków, Poland*
[3]*Space Radio-Diagnostics Research Centre, University of Warmia and Mazury, ul. Prawochenskiego 15, PL-10-720 Olsztyn, Poland*

ABSTRACT

We report the observations of single pulse emission from the pulsar B0809+74 at 150 MHz using the Polish LOFAR station, PL-611. The three major phenomena of subpulse drifting, nulling, and mode changing associated with single pulse variations are prominently seen in these observations. The pulsar has a single-component conal profile and the single pulses are primarily in the 'normal' drift mode with periodicity (P_3) 11.1 ± 0.5 P for 96 per cent of the observing duration, while the shorter duration 'slow-drift' mode has $P_3 = 15.7 \pm 1.2\ P$. We were able to measure the phase behaviour associated with drifting from the fluctuation spectral analysis that showed identical linear phase variations across the pulse window for both modes despite their different periodic behaviour. Earlier studies reported that the transitions from the normal state to the slow-drift mode were preceded by the presence of nulling with typical durations of 5 to 10 periods. Our observations however seem to suggest that the transition to nulling follows shortly after the pulsar switches to the slow-drift mode and not at the boundary between the modes, with one instance of complete absence of nulling between mode switching. In addition, we also detected a second type of short-duration nulls not associated with the mode changing that showed quasi-periodic behaviour with periodicity $P_N \sim 44 \pm 7$. The variety of features revealed in the single pulse sequence makes PSR B0809+74 an ideal candidate to understand the physical processes in the Partially Screened Gap dominated by non-dipolar magnetic fields.

Key words: pulsars: individual: PSR B0809+74.

1 INTRODUCTION

PSR B0809+74, one of the brightest pulsars seen over a wide frequency range, exhibits the three prominent phenomena associated with single pulse emission, viz. subpulse drifting, nulling, and mode changing, and as a result the radio emission from the pulsar has been widely studied (Vitkevich & Shitov 1970; Taylor & Huguenin 1971; Lyne & Ashworth 1983; van Leeuwen et al. 2002; Mitra & Rankin 2011; Gajjar, Joshi & Kramer 2012; Hassall et al. 2013). The pulsar has a single-component profile which bifurcates at the lowest frequency range below 100 MHz. The profile morphology and line of sight (LOS) geometry has been characterized in great detail (see Rankin & Rosen 2014, for a summary), and the pulsar profile has been classified as conal single (S_d), where the LOS cuts across the emission beam near its edge. The bifurcation at low frequencies is seen in many pulsars with S_d type profiles and is believed to be an effect of radius to frequency mapping, where the LOS cuts move away from the edge and towards the centre of the emission beam with decreasing frequency (Rankin 1983, 1993). The single pulse

emission shows prominent drift bands across the emission window and is an exemplar of the subpulse drifting phenomenon with multiple emission modes, along with other conal pulsars like PSR B0031−07 (Huguenin, Taylor & Troland 1970; Vivekanand & Joshi 1997; Smits, Mitra & Kuijpers 2005; McSweeney et al. 2017), PSR B0943+10 (Deshpande & Rankin 2001; Backus, Mitra & Rankin 2010; Bilous 2018), PSR B1819−22 (Basu & Mitra 2018b; Janagal et al. 2022), PSR B2303+30 (Redman, Wright & Rankin 2005), amongst others.

The drifting behaviour is characterized by the periodicity, P_3, that signifies the repetition time of subpulses along any longitude of the emission window. There are several methods of measuring P_3, primarily using the mathematical technique of Fast Fourier transform (FFT). The most commonly used method is the longitude resolved fluctuation spectra (LRFS, Backer 1973), where FFT is carried out for a series of pulse intensities along each longitude, and the drifting appears as a peak frequency ($f_p = 1/P_3$) in the fluctuation spectra, while the FFT phases corresponding to the peak amplitude measure the relative shift of the subpulses across the emission window. Other techniques also focus on estimating a second periodicity, P_2, the longitudinal separation between two adjacent drift bands, and represents an average estimate of the phase variations measured in the LRFS. These include the two-dimensional fluctuation spectrum (2DFS,

⋆ E-mail: r.basu@ia.uz.zgora.pl (RB); w.lewandowski@ia.uz.zgora.pl (WL); j.kijak@ia.uz.zgora.pl (JK)

Edwards & Stappers 2002) and the harmonic resolved fluctuation spectra (HRFS, Deshpande & Rankin 2001). The peak locations in both 2DFS and HRFS give estimates of P_3 as well as P_2. Other variants of these techniques are used to measure the temporal changes in the drifting behaviour by a continuous shift in the FFT sequence within the observing duration, both for the LRFS (Basu et al. 2016) and the 2DFS (S2DFS, Serylak, Stappers & Weltevrede 2009).

The single pulse emission properties of PSR B0809+74 has been studied in great detail by van Leeuwen et al. (2002), where a description of the drift-mode-null behaviour is provided. The pulsar is primarily seen in the 'normal' mode with prominent phase-modulated drifting which switches to the 'slow-drift' mode at certain instances with a longer P_3. It was reported that the boundary between the two modes are separated by nulls lasting between 5 and 10 periods. In addition, the pulsar also exhibits short-duration nulls lasting between one and two periods. Another relatively detailed study of the drifting behaviour in the normal mode was conducted by Hassall et al. (2013), where observations were carried out spanning two orders of magnitude in frequency, between 40 MHz and 5 GHz. The study found the drifting periodicity to be identical across the frequency range, but the phase variations of the subpulses within the emission window have detectable differences. At any given frequency the subpulses show non-linear phase variations across the emission window, i.e. the separation between two adjacent subpulses changes as a function of the longitude range. The phase variations across the emission window are also frequency-dependent, showing a gradual evolution in shape. It was noted in Hassall et al. (2013) that the non-linearity associated with the phase behaviour and its frequency evolution cannot be explained by the widely used model of subpulse drifting arising due to $\mathbf{E} \times \mathbf{B}$ of drift of sparking discharges in an inner vacuum gap above the dipolar polar cap (Ruderman & Sutherland 1975).

In recent years an updated understanding of the origin of subpulse drifting has been proposed based on the Partially Screened Gap model (PSG, Gil, Melikidze & Geppert 2003). It is expected that the inner vacuum gap is partially screened due to discharge of thermally generated ions from the heated polar cap surface. On the other hand detailed measurements show that the magnetic field structure above the polar cap is dominated by the non-dipolar component (Gil et al. 2008; Geppert 2017; Szary et al. 2017; Arumugasamy & Mitra 2019; Pétri & Mitra 2020; Sznajder & Geppert 2020). The sparks in the PSG are formed in a tightly packed configuration, lagging behind the rotation motion of the star which gives rise to the observed drifting behaviour (Basu, Mitra & Melikidze 2020a; Basu, Melikidze & Mitra 2022). The above model has been successful in explaining the non-linear drifting phase behaviour in certain pulsars (Basu, Mitra & Melikidze 2023). The non-linearity seen in the drifting phase behaviour of PSR B0809+74 is an ideal testbed to further investigate the applicability of the model of subpulse drifting from PSG. This was our initial motivation to carry out detailed observations of the single pulse emission from PSR B0809+74 using the Polish LOFAR station, PL-611 (Błaszkiewicz et al. 2018). However, in the process of analysing the single pulse behaviour we have found several previously unreported emission features associated with all three phenomena of mode changing, subpulse drifting, and nulling. As a result we have dedicated this work to report the single pulse properties of this pulsar at 150 MHz observing frequencies, while the detailed modelling of the subpulse drifting behaviour using the PSG model will be addressed in a separate paper. These results show that individual LOFAR stations are effective instruments to study single pulse emission from the brighter radio pulsars.

2 OBSERVATIONS AND ANALYSIS

The observations of PSR B0809+74 were carried out using Polish LOFAR station, PL-611, located in Łazy, near Krakow, which is part of the POLFAR Consortium (Błaszkiewicz et al. 2016, 2018). We used the HBA part of the telescope which operates around a centre frequency of 150 MHz with a bandwidth of 80 MHz. PSR B0809+74 forms part of a monitoring program with POLFAR, involving around 50–100 pulsars, to study the scintillation and scattering effects of the interstellar medium on pulsar signal. Each pulsar is observed for a duration of 1–2 h on roughly a monthly cadence. In these observations the pulsar signals are averaged over 10 s and therefore not suitable for single pulse studies. However, these measurements revealed high detection sensitivity for the 10 s integrated signals from PSR B0809+74, suggesting suitability of this object for single pulse studies with POLFAR.

The data were obtained using the LUMP software system[1] and coherently dedispersed offline to split into 366 frequency channels over a final bandwidth of 71.5 MHz, centred at 153.8 MHz observing frequency. Each pulse period was divided into 1024/2048 time bins and recorded individually before being combined into a single pulse sequence. We conducted separate observations to record the single pulse emission on two separate occasions, 2019 June 25, for roughly 3 h observing duration resulting in 8116 single pulses, and for roughly 5.5 h duration in 2022, resulting in 15 080 single pulses. The detection sensitivity reduced during the last third of the later observation limiting some of the single pulse studies to around 11 900 pulses. Subsequent analysis involved removing Radio Frequency Interference (RFI) across time and frequency channels as well as averaging over the bandwidth and were implemented using the PSRCHIVE package (van Straten, Demorest & Oslowski 2012) and specially designed RFI removal codes for POLFAR data analysis. Finally, single pulse stacks were produced comprising of two-dimensional representation with the rotation longitude along the x-axis and the pulse number in the y-axis. All subsequent single pulse analysis were carried out on the pulse stacks.

3 EMISSION PROPERTIES

3.1 Mode behaviour

The detailed mode behaviour of PSR B0809+74 has been known primarily from the studies reported in van Leeuwen et al. (2002). The authors used the Westerbork Synthesis Radio Telescope to observe the pulsar over a 18 month period, with around 3.6×10^4 measured single pulses. But individual observing sessions were short-lived and lasted less than 1000 pulses at a time and no detailed measurements of mode durations were reported. The pulsar was primarily found in the normal mode with prominent subpulse drifting. It was reported that slow drifting sequences start after the pulsar switches to nulls. In addition, the authors found two occasions, in 1999 and 2000, where the slow-drift mode lasted for longer durations of around 120 pulses.

The longer duration observations enabled us to study the mode statistics in more detail. The two emission modes could be clearly identified by visual inspection of the pulse stacks from the two observing sessions. A detailed breakdown of the individual mode sequence during each observing session is reported in Appendix A (see Table A1). Fig. 1 shows examples of the single pulse behaviour during the dominant normal mode (left panel) and transitions to the

---

[1]Developed by James Anderson, https://github.com/AHorneffer/lump-lofar-und-mpifr-pulsare.
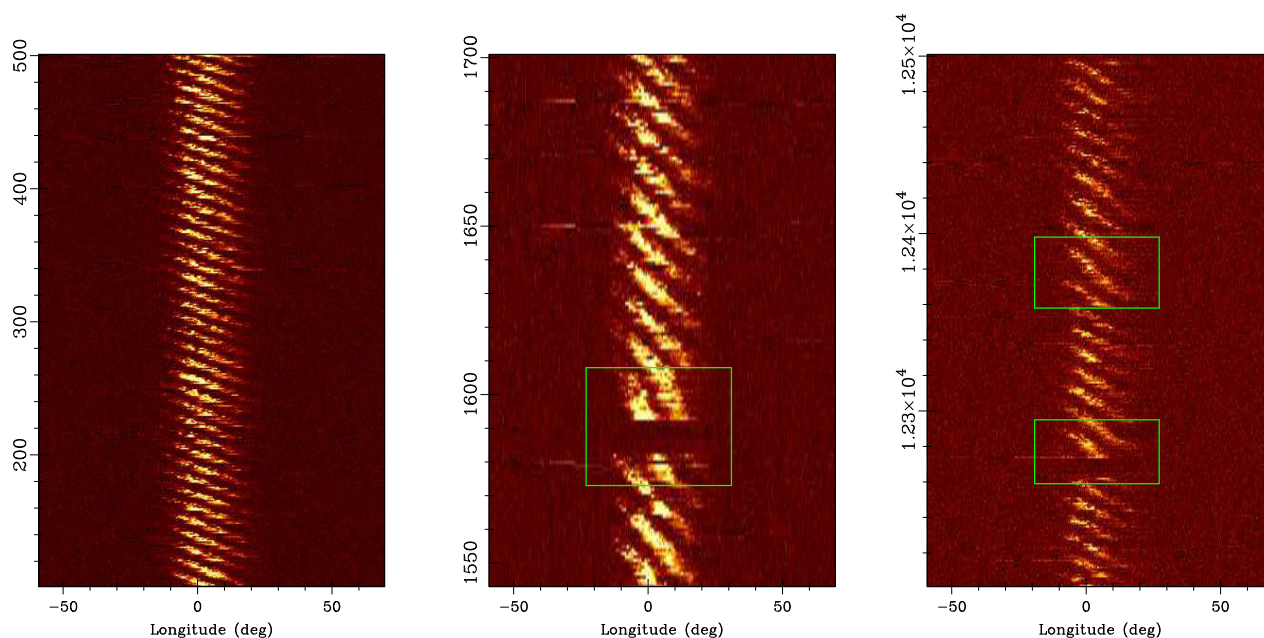
Figure 1. The figure shows three sequences of single pulse emission from PSR B0809+74 observed on 2022 October 7, representing the mode changing behaviour. The left panel shows a long sequence in the normal mode with prominent drift bands. The middle panel shows a transition from the normal mode to the slow-drift mode and back, where the box identifies the slow-drift mode. The switch from the normal mode to the slow-drift mode takes place around 10 periods before the pulsar switches to the longer null state. The drift information appears to be preserved across the long null lasting 10 periods. The right panel shows two instances of the mode transitions that closely follow each other, with the slow-drift mode once again identified within the boxes. The first mode transition is associated with the usual longer nulls closely following the transition to the slow-drift mode. However, no nulling event was seen during the second mode transition event.

Table 1. Statistics of the two emission modes.

| Date	N_p	N_T	Mode	Abundance (per cent)	Avg. length (P)
2019-06-25	8116	12	Normal	95.1	593.5
			Slow-drift	4.9	33.3
2022-10-07	15 080	12	Normal	96.5	1119.6
			Slow-drift	3.5	43.8
Full	23 196	24	Normal	96.0	856.6
			Slow-drift	4.4	38.6

slow-drift mode (middle and right panels). The normal mode showed prominent drift bands at 150 MHz similar to higher frequency behaviour. The single pulses in the slow-drift mode were comparatively brighter than the normal mode with much straighter drift bands. We found that the slow-drift mode is associated with nulling lasting between 3 and 11 periods at a time, as reported earlier. However, nulling is usually seen a few periods after the pulsar switches to the slow-drift mode (see Fig. 1, middle panel) and does not form the boundary between the two emission modes, contrary to previous reports. In one instance nulling was entirely absent when the pulsar emission switched from the normal mode to slow-drift mode and back (see Fig. 1, right panel).

There were 12 transitions between the emission modes observed on each of the observing sessions. The average statistics of the modes are summarized in Table 1. The normal mode was dominant and seen for 96 per cent of the observing duration. The mode duration distribution is shown in Fig. 2 (left panel), and had large variations between 31 and 3312 periods, with typical values in the range 500–600P. We did not detect the longer duration slow-drift modes lasting more than 100P, reported in van Leeuwen et al. (2002). The distribution of the

mode lengths is also shown in Fig. 2 (right panel), and had relatively less spread varying between 21 and 85 periods. There were only two instances when the mode length exceeded 50P and the slow-drift mode had typical durations lasting 30–40P. The longer duration nulls seen within the slow-drift mode usually lasted between 3 and 11P (see Table A1). The slow-drift mode was seen for short durations of 5–12P before the onset of the nulls and could be identified due to their increased intensities (see Fig. 3) and change in the drift behaviour. The mode changing in this pulsar seems to show certain evolution with time, with the presence of longer duration slow-drift mode reported in earlier studies, as well as the slow-drift mode being more frequent during the 2019 observations compared to the 2022 observations. However, characterizing the details of the time evolution of the mode changing behaviour will require regular, more evenly spaced observations.

3.1.1 Average profile

The average profile of the pulsar shows a single-component typical of the conal single classification (Rankin 1993), but exhibits an asymmetric nature with absorption like feature towards the trailing side which has also prompted the profile to be termed a 'partial cone' (Mitra & Rankin 2011). The average profiles of the two emission modes are shown in Fig. 3, left panel, where the normal mode has the asymmetric nature, while the slow-drift mode is more symmetric and seen prominently towards the trailing side as well. The average profile properties are reported in Table 2, including the widths W_{50} and W_{10}, measured at 50 per cent and 10 per cent of the peak intensity level, respectively, and $W_{5\sigma}$ which specifies the emission window by estimating the widths above five times the baseline noise rms levels. The relative intensities of the profiles show that the slow-drift mode is brighter than the normal mode, with the peak intensity being around
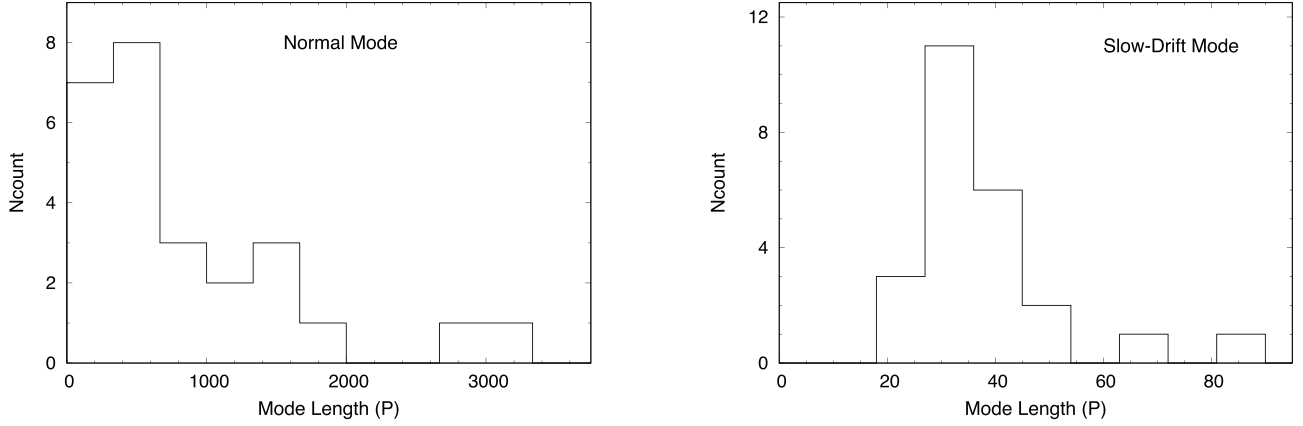
Figure 2. The left panel shows the distribution of the mode lengths during the normal state, while the right panel shows the distribution of the durations of the slow-drift mode. Both distributions have been estimated by combining the observations on 2019 June 25 and 2022 October 7.
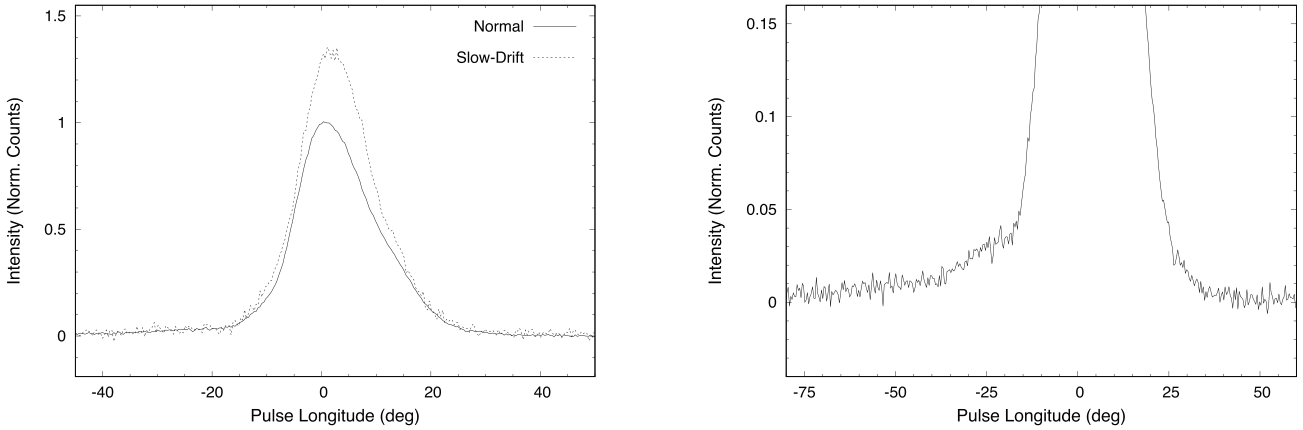
Figure 3. The left panel shows the folded profiles of the normal mode and the slow-drift mode. The right panel shows the zoomed baseline of the average profile showing low-level emission at the leading edge.

Table 2. Average profile properties.

| | W_{50} (°) | W_{10} (°) | $W_{5\sigma}$ (°) | Int. ratio | |
				Peak int.	Avg. int.
Normal	17.9 ± 0.9	35.9 ± 0.9	88.6 ± 0.9	1.0	1.0
Slow-drift	16.9 ± 0.9	34.8 ± 0.9	40.7 ± 0.9	1.34 ± 0.01	1.29 ± 0.01
Full	17.9 ± 0.9	35.9 ± 0.9	89.6 ± 0.9	–	–

35 per cent higher in the slow-drift mode compared to the normal mode, while the average energy of slow-drift mode being around 30 per cent brighter.

The W_{50} and W_{10} measurements in the two modes match within errors which suggests that the location of the emission region remains largely unchanged during mode changing (Basu & Mitra 2018b; Basu, Paul & Mitra 2019b; Rahaman et al. 2021). The right panel of Fig. 3 shows the zoomed-in baseline region of the normal mode profile and shows low-level emission at the trailing side of the profile, extending from around $-40°$ till $-15°$ from the profile peak. This is further evidenced by the large value of $W_{5\sigma}$ for this profile, which is more than twice the W_{10} value. The extended feature is not visible in the slow-drift mode profile due to higher baseline noise levels. A second component in the pulsar profile becomes prominent at frequencies below 100 MHz (Hassall et al. 2012) and it is one possibility that the component starts becoming visible at low levels

from 150 MHz. However, in these earlier works the pulsar profile shows a wide evolution with frequency where a second component becomes visible at frequencies above 1 GHz in addition to the bifurcation of the profile below 100 MHz. It has been suggested that at low frequencies the second component appears at the trailing side, while the high-frequency second component is at the leading side, and can be considered a distinct third component feature. Taking into account this interpretation the low-level emission at the leading edge can very well be the remnants of the second (third) component from the high-frequency profiles.

3.2 Subpulse drifting

The two emission modes show visible drift bands that were studied using the LRFS. Fig. 4 shows the LRFS of three pulse sequences observed on 2022 October 7, corresponding to the normal mode
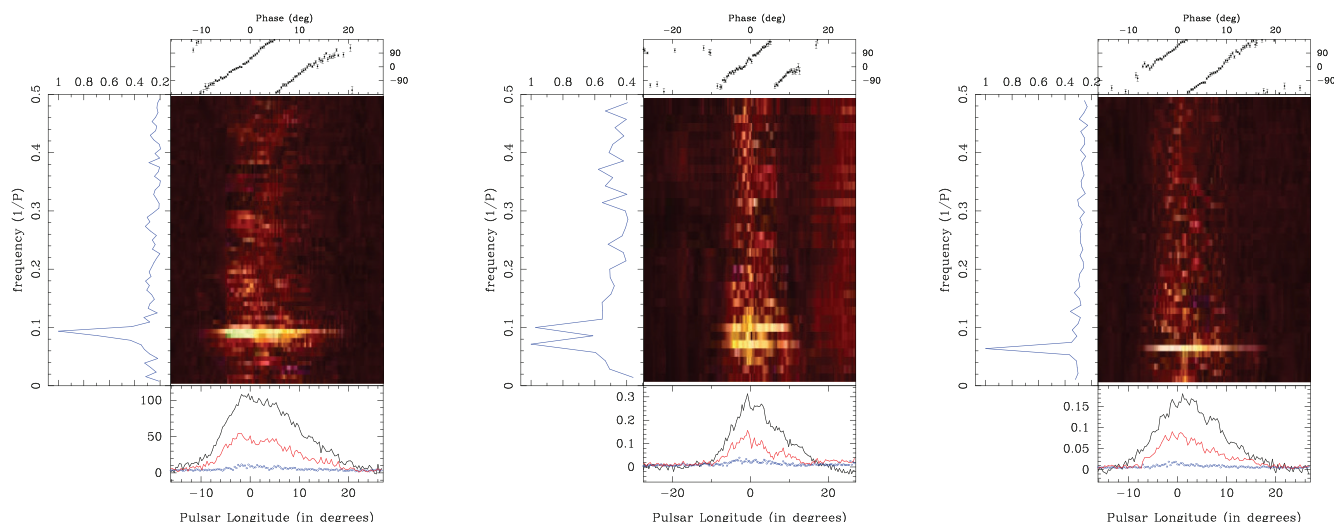
Figure 4. The figure shows the LRFS from three different single pulse sequences showing the drifting behaviour in the two emission modes of PSR B0809+74 at 150 MHz. The left panel shows the LRFS of the normal mode with one clear frequency peak due to the prominent subpulse drifting behaviour. The central panel corresponds to a pulse sequence containing both emission modes and shows the two peaks, the lower peak of the slow-drift mode, and the higher peak from the normal mode. The right panel shows the LRFS for a sequence in the slow-drift mode.

Table 3. Subpulse drifting measurements.

	f_p (cy/P)	FWHM (cy/P)	P_3 (P)	Phase slope (°/°)
Normal	0.090 ± 0.004	0.0093	11.1 ± 0.5	23.19 ± 0.06
Slow-drift	0.064 ± 0.005	0.012	15.7 ± 1.25	25.1 ± 0.2

(left panel), an overlapping region with both modes present (middle panel) and the slow-drifting mode (right panel). The different drifting behaviour in the two modes is highlighted by their different periodic behaviour, with clearly separated peak frequencies seen in the middle panel of the figure. The lower frequency represents the longer drifting periodicity of the slow-drift mode, while the higher frequency feature signify the periodic behaviour of the normal mode. The normal mode usually has longer durations, lasting for several hundred periods at a time, and the average fluctuation spectra for all such sections was estimated to find the drifting periodicity as well as the phase behaviour. The average behaviour was obtained by estimating the LRFS corresponding to 256 consecutive pulses at a time and subsequently shifting the starting point by 50 periods (see Basu et al. 2016; Basu & Mitra 2018a, for details). On the other hand clear measurements of drifting behaviour, particularly the phase variations, were only possible in the slow-drift mode where the two longer sequences exceeded 50 pulses.

Table 3 reports the drifting measurements from the two emission modes, which include the frequency peak, f_p, of drifting in the LRFS, the full width at half-maximum (FWHM) of the frequency feature, the drifting periodicity, P_3, and the slope of the drifting phase variations. The P_3 measured from the LRFS is $11.1 \pm 0.5P$ in the normal mode and $15.7 \pm 1.25\ P$, which agrees with earlier estimates (van Leeuwen et al. 2002). Fig. 5 shows the phase variations across the emission window associated with subpulse drifting in the two emission modes. The phase behaviour of the normal mode has been studied in earlier works (Hassall et al. 2013), and we find a mostly linear phase variation from the leading to the trailing edge of the emission window with a positive slope of 23.19 ± 0.06 °/° from the average LRFS estimate (see green points in Fig. 5). In contrast, the
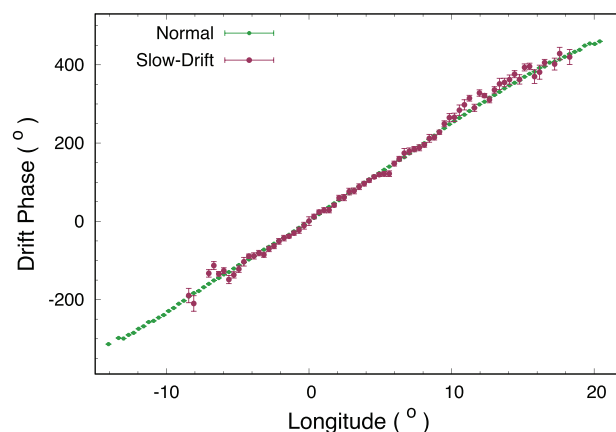

Figure 5. The phase behaviour associated with subpulse drifting in the two emission modes. The average phase behaviour of the normal mode is shown from the entire duration of the observation, while the phase behaviour of the slow-drift mode corresponds to one instance, between pulse number 12 355 and 12 440 on 2022 October 7, where these measurements were possible.

drift phase variations of the slow-drift mode has not been reported in earlier works. Our estimates show (red points in Fig. 5) that the phase behaviour in slow-drift mode closely follows the linear phase behaviour of the normal mode with positive slope of 25.1 ± 0.2 °/°, with possible small deviations near the trailing side of the profile, despite the P_3 in this mode being almost 50 per cent longer than the normal mode.

3.3 Nulling

The pulsar emission shows the presence of longer duration nulls, lasting between 3 and 11 periods at a time, shortly after the pulsar transitions to the slow-drift mode (see Section 3.1 and also Table A1). In addition, we have also found the single pulse sequences on both observing sessions to show frequent transition to short-duration nulls usually lasting one or two periods at a time. Hence, we report the presence of two distinct category of nulling behaviour in PSR
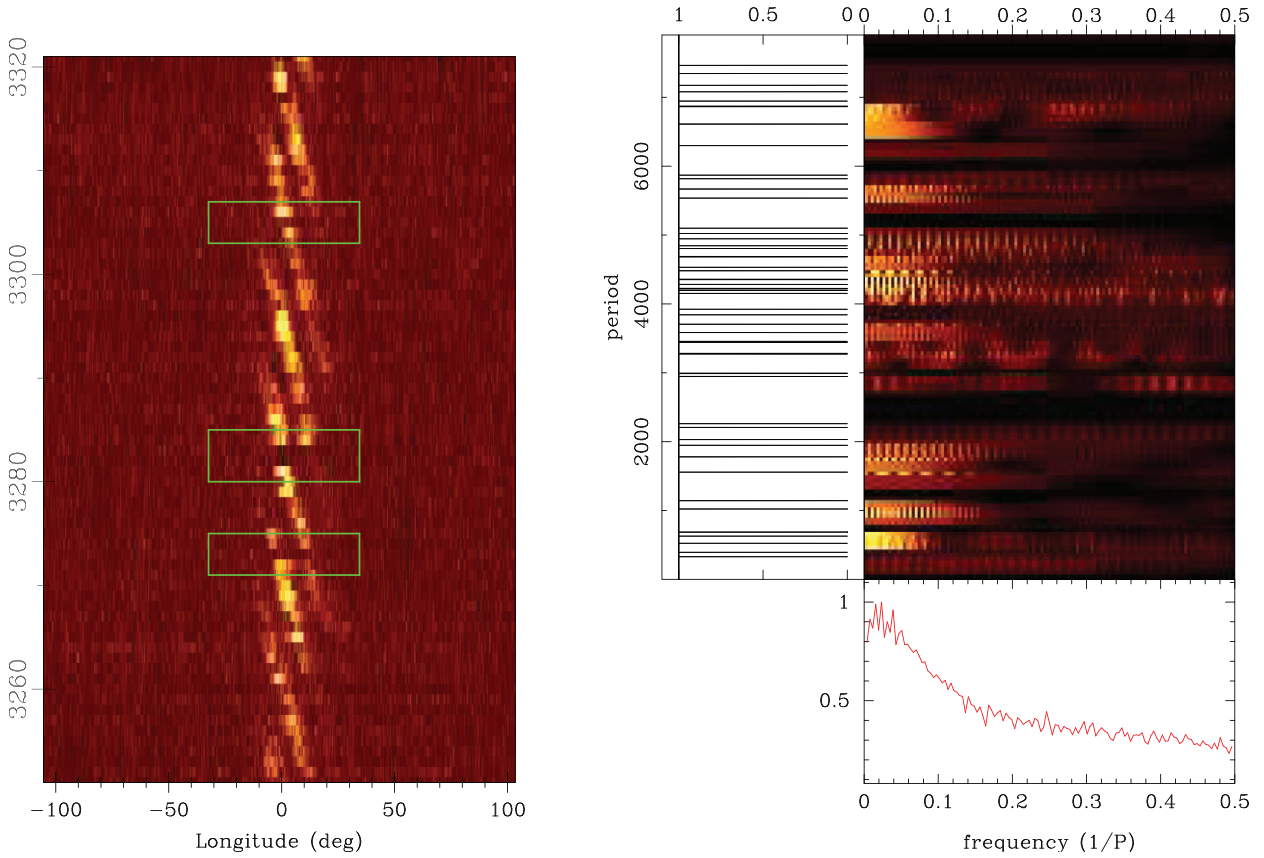
Figure 6. The left panel shows three examples of short-duration nulling (shown in boxes) seen in short succession, in the single pulse sequence observed on 2019 June 25, at pulse number 3273, pulse numbers 3282 and 3283, and pulse number 3305. The right panel shows the FFT analysis of the binary sequence where the nulls are identified as '0' and bursts as '1'. This binary series shows a wide, low-frequency peak in the FFT, signifying the periodic nulling behaviour in PSR B0809+74.

Table 4. Nulling characteristics.

	N_T	$\langle BL \rangle$ (P)	$\langle NL \rangle$ (P)	NF (per cent)	η	P_N (P)
All	147	130.0	2.1	1.56 ± 0.09	928.8	44.3 ± 7.0
Mode	20	–	6.5	0.62 ± 0.06	–	–
Short	127	–	1.5	0.94 ± 0.07	–	–

B0809+74. Fig. 6 (left panel) shows an example of the short-duration nulls with three instances of transition from null to the burst state at short succession. We have carried out detailed analysis to characterize the nature of the two different nulling behaviour seen in the single pulse sequence. The nulling measurements are usually carried out by finding statistical cut-offs between the null and the burst pulses and therefore require the single pulse emission to be measured with high detection sensitivity. The single pulse detection sensitivity degraded towards the last third of the observing session on 2022 October 7, and we used the first 11 900 pulses for the nulling analysis. However, this did not affect the visual identification of the emission modes in this duration. No such issue was encountered during the first observing session on 2019 June 25.

The nulling behaviour in PSR B0809+74 is reported in Table 4, where the measurements from both observing sessions have been combined. The nulling fraction (*NF*) measures the percentage of time the emission is in the null state and was estimated to be 1.56 ± 0.09 per cent, which agrees with previous measurements (van Leeuwen

et al. 2002; Gajjar et al. 2012). Within the measurement window covering both observing sessions we found a total of 147 transitions from the null to the burst state and back. Out of these, the majority of nulling, around 85 per cent (127), were short-lived usually lasting one or two periods, while around 15 per cent (20) of nulling events were of longer duration, lasting between 3 and 11 periods, and were linked with the mode changing behaviour. The null length and burst length distributions are shown in Fig. 7, which further highlights the preponderance of the short-duration nulls. The average length of the short nulls ($\langle NL \rangle$) was around $1.5P$, while the longer nulls associated with the slow-drift mode had average duration of $6.5P$. However, due to the relatively longer lengths the mode associated nulls made up around 40 per cent ($NF = 0.62 \pm 0.06$ per cent) of the total null pulses, while the short-duration nulls comprised the remaining 60 per cent ($NF = 0.94 \pm 0.07$ per cent). The burst lengths showed wide variations ranging from few tens of periods (see Fig. 6, left panel) to several hundred periods at a time, with a mean length, $\langle BL \rangle = 130P$.

The null pulses were averaged to form the null profile in Fig. 8, lower panel, that has noise-like behaviour in the pulse window, indicating the absence of any low-level emission during nulling. The degree of decline of the radio emission during the null state, η, can be obtained from the null and the burst profiles (Fig. 8, upper panel) as $\eta = \Sigma P(i)/3\sigma_N$. Here, $P(i)$ is the intensity at the ith longitude bin of the burst profile window, while σ_N is the noise rms in the emission window of the null profile. We estimated $\eta = 928.8$, which is an improvement of more than a factor of 5 higher than previously
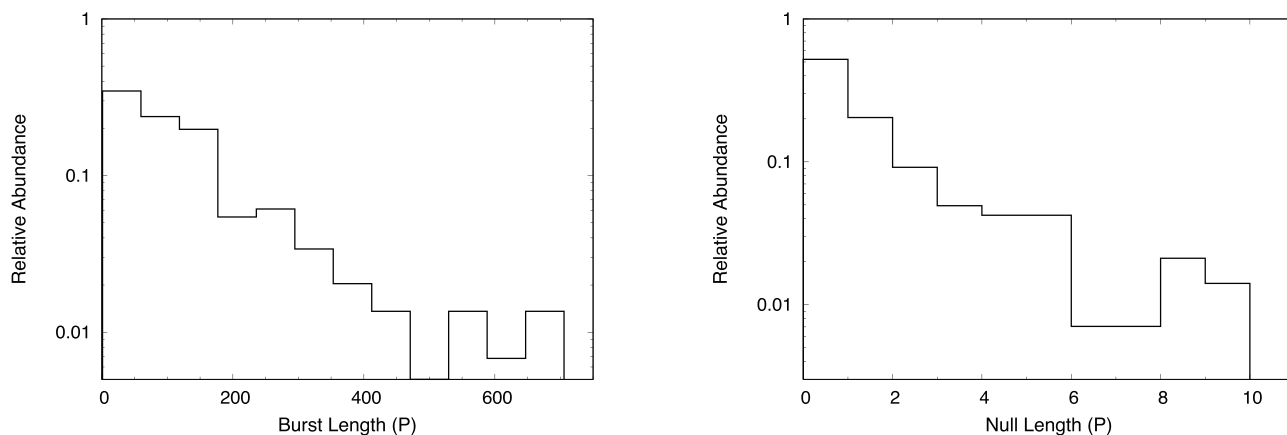
Figure 7. The left panel shows the distribution of the duration of the burst sequences obtained from both observing sessions. The right panel shows the corresponding distribution for the null sequence.
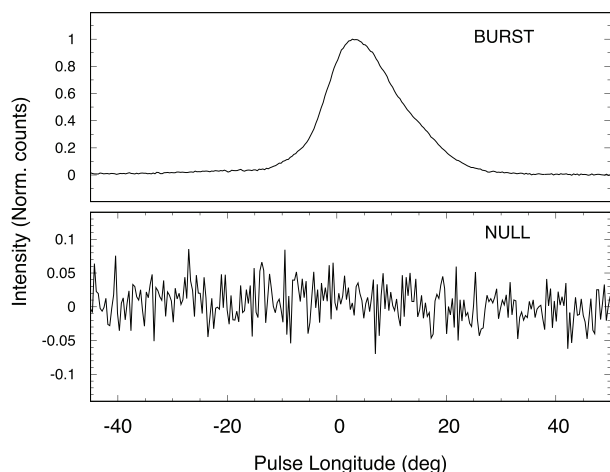
Figure 8. The figure shows the average profiles obtained from the Burst and Null pulses from the observations on 2019 June 25.

reported (Gajjar et al. 2012), and highlights that there is significant reduction in the emission level during nulling.

Finally, we have also studied the presence of periodic modulations associated with the nulling behaviour. We followed the analysis scheme developed by Basu, Mitra & Melikidze (2017), where the single pulse sequence was converted into a binary series with the null pulses identified as '0' and the burst pulses as '1'. A time-varying FFT of this series was carried out for 256 pulses at a time and subsequently shifting the starting point by 50 periods. The FFT from the null-burst time sequence for the observations on 2019 June 25 is shown in Fig. 6, right panel, and has a wide low-frequency feature. This demonstrates that in addition to subpulse drifting, PSR B0809+74 also shows periodic nulling with periodicity, $P_N = 44.3 \pm 7.0P$. The periodic nulling behaviour is usually hidden in the LRFS due to the strong drifting feature and is clearly revealed in the binary sequence, where the drifting information is suppressed. The periodic nulling behaviour is primarily a feature of the short-duration nulls which dominate the null to burst transitions.

4 DISCUSSION

In this work, we have presented the results of the single pulse observations of PSR B0809+74 conducted with the Polish LOFAR

station, PL-611, located near Krakow. Our results confirm that individual stations of the LOFAR telescope are capable of detecting single pulse with high sensitivity, at least from several of the brighter pulsars. It is worth noting that the PL-611 station operates in the so-called 'remote station' configuration, where only a half of the usual international station's HBA antennas (48 instead of 96) is present, but is still sufficiently sensitive for the single pulse studies.

PSR B0809+74 is a well-known example showing the three distinct phenomena of subpulse drifting, nulling, and mode changing in the pulse sequence. In addition, we have also detected periodic nulling which is a form of periodic modulation, a distinct emission feature seen in around 30 pulsars (Basu, Mitra & Melikidze 2020c). The pulsar joins a select group of sources where the periodic nulling coexist with subpulse drifting as well as multiple emission modes in the pulse sequence, with other prominent examples being PSR B0031−07 (Basu et al. 2017), PSR B1819−22 (Basu & Mitra 2018b), PSR B1918+19 (Herfindal & Rankin 2009), PSR B2000+40 (Basu, Lewandowski & Kijak 2020b), PSR B2003−08 (Basu et al. 2019b), PSR B2319+60 (Rahaman et al. 2021), etc. PSR B0809+74 is further distinguished by the presence of two different types of nulls, the longer duration nulls associated with the slow-drift mode, and more frequent short-duration nulls that contribute to periodic behaviour.

The physical mechanism governing the frequent transitions between the emission modes and the periodic nulling behaviour is not well understood. There have been suggestions that the change in the underlying magnetic field configurations near the polar cap region can modify the plasma generation process, leading to variations in the emission properties. A possible mechanism for such changes in the form of perturbations introduced to the polar cap magnetic field by the Hall drift and thermoelectrically driven magnetic field oscillations has been suggested (Geppert et al. 2021). But more work is required to understand the nature of changes in the surface field due to such effects as well as the corresponding effect on the radio emission, before they can be used to explain the observed behaviour.

The underlying mechanism of the subpulse drifting behaviour on the other hand has been studied in more detail. The plasma responsible for the radio emission in pulsars is expected to arise due to sparking discharges from electron–positron pair production in an inner acceleration region (IAR) above the polar cap, which was initially modelled as a vacuum gap (Ruderman & Sutherland 1975). During the sparking process the plasma lag behind the rotation of the star due to **ExB** drift in the IAR. The spark generated plasma

subsequently populate the open field line region and give rise to the radio emission (Melikidze, Gil & Pataraya 2000; Gil, Lyubarsky & Melikidze 2004), where the lagging behind rotation is imprinted and observed as subpulse drifting. Several attempts have been made to understand the drifting behaviour in pulsars based on the vacuum gap model, where the magnetic field is considered to be dipolar in nature in the polar cap region, and the sparks are expected to rotate around the magnetic axis in the form of a carousel (Gil & Sendyk 2000). The non-linear behaviour of the drifting phase variations across the emission window and their frequency evolution has been particularly challenging to address using the above mechanism. The geometric model of Edwards & Stappers (2002) can explain the non-linear behaviour in certain pulsars with deviations from linearity near the profile edges. However, an increasing number of pulsars have been found to show complex phase behaviour like bi-drifting, where different components of the profile show reversal in the direction of phase variations (Champion et al. 2005; Weltevrede 2016; Szary & van Leeuwen 2017; Basu & Mitra 2018a; Basu et al. 2019b; Szary et al. 2020; Shang et al. 2022), large phase jumps between adjacent components (Basu et al. 2016, 2019a), etc., which are difficult to understand using this model. Several complex scenarios, such as the presence of two different carousel motions with frequency-dependent delays (Hassall et al. 2013; Rankin & Rosen 2014), tilted elliptical beams (Wright & Weltevrede 2017), etc., have been proposed to explain some of these observed behaviour, although it is unclear what the physical origin of such configurations are within a vacuum gap model.

An updated model of subpulse drifting has been proposed recently based on the PSG model of the IAR, where the backstreaming electrons heat the polar cap surface to high temperatures, such that positively charges ions can flow freely from the surface to partially screen the potential difference along the IAR (Gil et al. 2003). The polar cap region in a PSG is expected to be dominated by highly non-dipolar magnetic fields, while the emission region has dipolar magnetic fields (Gil, Melikidze & Mitra 2002). In such a configuration the sparks lag behind the rotation motion of the pulsar and are constrained by the open field line boundary to exhibit two distinct drift patterns, along the clockwise and counterclockwise directions around a stationary central spark, in the two halves of the polar cap (Basu et al. 2020a, 2022). The phase behaviour of subpulse drifting traces the evolution of the sparking pattern along the LOS of the observer. Since the LOS cuts across the emission beam, the non-linear phase behaviour of subpulse drifting naturally arises as the magnetic field lines transition from the non-dipolar fields in the IAR to the dipolar fields higher up in the emission region. The above model has been used to find appropriate orientation of the surface magnetic field structure and reproduce the observed non-linear drifting phase variations in two pulsars, PSR J1034−3224 and PSR B1717−29 (Basu et al. 2023). We intend to extend these studies to the drifting behaviour of PSR B0809+74 in a future work.

The drifting phase behaviour is expected to change as a function of frequency due to the effect of radius to frequency mapping, where the lower frequencies arise from higher up the open dipolar field line region (Kijak & Gil 2003). Further constraints are provided by the variations of the drifting behaviour during mode changing. The slow-drift mode has a periodicity which is around 50 per cent longer than the normal mode. In the PSG model the drifting periodicity is inversely proportional to the screening factor in the IAR (Basu et al. 2020a; Mitra et al. 2020). Hence, an increase in the drifting periodicity requires changes in the screening condition, which are governed by several factors including the surface magnetic field strength. On the other hand the phase behaviour of the slow-

drift mode closely follow the normal mode, suggesting that the relative orientation of the surface magnetic fields with respect to the LOS remains unchanged in the two emission modes. Thus the surface magnetic field strength changes without affecting its relative orientation, and needs to be accounted for while modelling the drifting behaviour.

ACKNOWLEDGEMENTS

DATA AVAILABILITY

The data underlying this article will be shared on reasonable request to the corresponding author.

REFERENCES

Arumugasamy P., Mitra D., 2019, MNRAS, 489, 4589
Backer D. C., 1973, ApJ, 182, 245
Backus I., Mitra D., Rankin J. M., 2010, MNRAS, 404, 30
Basu R., Mitra D., 2018a, MNRAS, 475, 5098
Basu R., Mitra D., 2018b, MNRAS, 476, 1345
Basu R., Mitra D., Melikidze G. I., Maciesiak K., Skrzypczak A., Szary A., 2016, ApJ, 833, 29
Basu R., Mitra D., Melikidze G. I., 2017, ApJ, 846, 109
Basu R., Mitra D., Melikidze G. I., Skrzypczak A., 2019a, MNRAS, 482, 3757
Basu R., Paul A., Mitra D., 2019b, MNRAS, 486, 5216
Basu R., Mitra D., Melikidze G. I., 2020a, MNRAS, 496, 465
Basu R., Lewandowski W., Kijak J., 2020b, MNRAS, 499, 906
Basu R., Mitra D., Melikidze G. I., 2020c, ApJ, 889, 133
Basu R., Melikidze G. I., Mitra D., 2022, ApJ, 936, 35
Basu R., Mitra D., Melikidze G. I., 2023, ApJ, 947, 86
Bilous A. V., 2018, A&A, 616, A119
Błaszkiewicz L., Lewandowski W., Krankowski A., Kijak J., Koralewska O., Dąbrowski B. P., 2016, Acta Geophys., 64, 293
Błaszkiewicz L. P. et al., 2018, Adv. Space Res., 62, 1904
Champion D. J. et al., 2005, MNRAS, 363, 929
Deshpande A. A., Rankin J. M., 2001, MNRAS, 322, 438
Edwards R. T., Stappers B. W., 2002, A&A, 393, 733
Gajjar V., Joshi B. C., Kramer M., 2012, MNRAS, 424, 1197
Geppert U., 2017, J. Astrophys. Astron., 38, 46
Geppert U., Basu R., Mitra D., Melikidze G. I., Szkudlarek M., 2021, MNRAS, 504, 5741
Gil J. A., Sendyk M., 2000, ApJ, 541, 351
Gil J. A., Melikidze G. I., Mitra D., 2002, A&A, 388, 235
Gil J., Melikidze G. I., Geppert U., 2003, A&A, 407, 315
Gil J., Lyubarsky Y., Melikidze G. I., 2004, ApJ, 600, 872
Gil J., Haberl F., Melikidze G., Geppert U., Zhang B., Melikidze G. J., 2008, ApJ, 686, 497
Hassall T. E. et al., 2012, A&A, 543, A66
Hassall T. E. et al., 2013, A&A, 552, A61
Herfindal J. L., Rankin J. M., 2009, MNRAS, 393, 1391
Huguenin G. R., Taylor J. H., Troland T. H., 1970, ApJ, 162, 727
Janagal P., Chakraborty M., Bhat N. D. R., Bhattacharyya B., McSweeney S. J., 2022, MNRAS, 509, 4573

Kijak J., Gil J., 2003, A&A, 397, 969
Lyne A. G., Ashworth M., 1983, MNRAS, 204, 519
McSweeney S. J., Bhat N. D. R., Tremblay S. E., Deshpande A. A., Ord S. M., 2017, ApJ, 836, 224
Melikidze G. I., Gil J. A., Pataraya A. D., 2000, ApJ, 544, 1081
Mitra D., Rankin J. M., 2011, ApJ, 727, 92
Mitra D., Basu R., Melikidze G. I., Arjunwadkar M., 2020, MNRAS, 492, 2468
Pétri J., Mitra D., 2020, MNRAS, 491, 80
Rahaman S. k. M., Basu R., Mitra D., Melikidze G. I., 2021, MNRAS, 500, 4139
Rankin J. M., 1983, ApJ, 274, 333
Rankin J. M., 1993, ApJ, 405, 285
Rankin J., Rosen R., 2014, MNRAS, 439, 3860
Redman S. L., Wright G. A. E., Rankin J. M., 2005, MNRAS, 357, 859
Ruderman M. A., Sutherland P. G., 1975, ApJ, 196, 51
Serylak M., Stappers B. W., Weltevrede P., 2009, A&A, 506, 865
Shang L.-H., Bai J.-T., Dang S.-J., Zhi Q.-J., 2022, Res. Astron. Astrophys., 22, 025018
Smits J. M., Mitra D., Kuijpers J., 2005, A&A, 440, 683
Szary A., van Leeuwen J., 2017, ApJ, 845, 95
Szary A., Gil J., Zhang B., Haberl F., Melikidze G. I., Geppert U., Mitra D., Xu R.-X., 2017, ApJ, 835, 178
Szary A., van Leeuwen J., Weltevrede P., Maan Y., 2020, ApJ, 896, 168
Sznajder M., Geppert U., 2020, MNRAS, 493, 3770
Taylor J. H., Huguenin G. R., 1971, ApJ, 167, 273
van Leeuwen A. G. J., Kouwenhoven M. L. A., Ramachandran R., Rankin J. M., Stappers B. W., 2002, A&A, 387, 169
van Straten W., Demorest P., Oslowski S., 2012, Astron. Res. Technol., 9, 237
Vitkevich V. V., Shitov Y. P., 1970, Nature, 225, 248
Vivekanand M., Joshi B. C., 1997, ApJ, 477, 431
Weltevrede P., 2016, A&A, 590, A109
Wright G., Weltevrede P., 2017, MNRAS, 464, 2597

APPENDIX A: EMISSION MODE SEQUENCE

A detailed list of pulse sequence in each emission mode is reported in Table A1. We also show the longer null intervals within the slow-drift mode.

Table A1. Emission mode sequence.

	2019 June 25					2022 October 7			
Mode	Pulse range (P)	Length (P)	Null (P)	Length (P)	Mode	Pulse range (P)	Length (P)	Null (P)	Length (P)
Normal	1–679	679			Normal	1–1573	1573		
Slow-drift	680–711	32	684–691	8	Slow-drift	1574–1606	33	1583–1592	10
Normal	712–1137	426			Normal	1607–2302	696		
Slow-drift	1138–1165	28	1142–1146	5	Slow-drift	2303–2349	47	2316–2324	9
Normal	1166–1769	604			Normal	2350–3906	1557		
Slow-drift	1770–1806	37	1778–1783	6	Slow-drift	3907–3946	40	3914–3923	10
Normal	1807–1941	135			Normal	3947–7258	3312		
Slow-drift	1942–1974	33	1946–1949	4	Slow-drift	7259–7293	35	7266–7271	6
Normal	1975–3691	1717			Normal	7294–7957	664		
Slow-drift	3692–3719	28	3704–3707	4	Slow-drift	7958–8005	48	7963–7967	5
Normal	3720–4345	626			Normal	8006–9089	1084		
Slow-drift	4346–4386	41	4352–4355	4	Slow-drift	9090–9122	33	9097–9103	7
Normal	4387–4472	86			Normal	9123–9246	124		
Slow-drift	4473–4506	34	4479–4484	6	Slow-drift	9247–9279	33	9252–9256	5
Normal	4507–4678	172			Normal	9280–9356	78		
Slow-drift	4679–4713	35	4686–4689	4	Slow-drift	9357–9378	22	9360–9364	5
Normal	4714–5092	379			Normal	9379–12 252	2874		
Slow-drift	5093–5116	24	5099–5101	3	Slow-drift	12 253–12 324	72	12 263–12 273	11
Normal	5117–5659	543			Normal	12 325–12 355	31		
Slow-drift	5660–5686	27	5665–5670	6	Slow-drift	12 356–12 441	86	–	0
Normal	5687–6603	917			Normal	12 442–12 992	551		
Slow-drift	6604–6640	37	6609–6614	6	Slow-drift	12 993–13 025	33	13 001–13 006	6
Normal	6641–6857	217			Normal	13 026–14 448	1423		
Slow-drift	6858–6901	44	6863–6871	9	Slow-drift	14 449–14 492	44	14 458–14 465	8
Normal	6902–8116	1215			Normal	14 493–15 080	588		

This paper has been typeset from a TeX/LaTeX file prepared by the author.